Strain and order-parameter coupling in Ni-Mn-Ga Heusler alloys from resonant ultrasound spectroscopy

C. Salazar Mejía,[1,*] N.-O. Born,[1] J. A. Schiemer,[2] C. Felser,[1] M. A. Carpenter,[2] and M. Nicklas[1,†]

[1]*Max Planck Institute for Chemical Physics of Solids, Nöthnitzer Str. 40, 01187 Dresden, Germany*
[2]*Department of Earth Sciences, University of Cambridge, Downing Street, Cambridge CB2 3EQ, United Kingdom*

Resonant ultrasound spectroscopy and magnetic susceptibility experiments have been used to characterize strain coupling phenomena associated with structural and magnetic properties of the shape-memory Heusler alloy series $Ni_{50+x}Mn_{25-x}Ga_{25}$ ($x = 0$, 2.5, 5.0, and 7.5). All samples exhibit a martensitic transformation at temperature T_M and ferromagnetic ordering at temperature T_C, while the pure end member ($x = 0$) also has a premartensitic transition at T_{PM}, giving four different scenarios: $T_C > T_{PM} > T_M$, $T_C > T_M$ without premartensitic transition, $T_C \approx T_M$, and $T_C < T_M$. Fundamental differences in elastic properties, i.e., stiffening versus softening, are explained in terms of coupling of shear strains with three discrete order parameters relating to magnetic ordering, a soft mode, and the electronic instability responsible for the large strains typical of martensitic transitions. Linear-quadratic or biquadratic coupling between these order parameters, either directly or indirectly via the common strains, is then used to explain the stabilities of the different structures. Acoustic losses are attributed to critical slowing down at the premartensite transition, to the mobility of interphases between coexisting phases at the martensitic transition, and to mobility of some aspect of the twin walls under applied stress down to the lowest temperatures at which measurements were made.

I. INTRODUCTION

Ni-Mn-Ga alloys that undergo a martensitic transformation, exhibit a shape-memory effect, specifically, a magnetic field induced structural reorientation. Large deformation values up to 12% in low magnetic fields have been reported [1]. Shape-memory materials, more generally, can be used in applications including as actuators and sensors or for energy harvesting [2]. Additionally, the materials of this family can exhibit a giant magnetocaloric effect [3]. The study of the lattice dynamics which underpin the martensitic transformations and their characteristic strain behavior is important for a deeper understanding of the physical mechanisms behind the multi-functional properties of these materials. Resonant ultrasound spectroscopy (RUS) gives information on the coupling of the order parameter with strain but also on relaxation phenomena [4]. Previous studies with RUS, or similar techniques, on different Ni-Mn-Ga samples have focused on the premartensitic transition, the damping properties, and the determination of the elastic constants of the alloys [5–11]. RUS experiments in magnetic field have been used to evaluate magnetoelastic properties in Ni_2MnGa [12–14]. Nevertheless, a combined systematic RUS and magnetic susceptibility study investigating the magnetostructural properties at the ferromagnetic, martensitic, and premartensitic transitions is still missing.

In this work, we have studied polycrystalline $Ni_{50+x}Mn_{25-x}Ga_{25}$ Heusler alloys with $x = 0$, 2.5, 5.0, and 7.5 using RUS and magnetic susceptibility measurements to focus on the temperature range which includes the ferromagnetic and the martensitic phase transitions. The selected concentrations belong to characteristically different groups in the $Ni_{50+x}Mn_{25-x}Ga_{25}$ phase diagram displayed in Fig. 1 [7,15–20]. The sample with $x = 0$ belongs to group I, in which the ferromagnetic transition occurs at values of T_C that are substantially above the martensitic transition temperature T_M and in which there is an intermediate field of stability for the premartensite structure $T_C > T_{PM} > T_M$. The sample with $x = 2.5$ belongs to group II, in which T_M is close to room temperature, still below T_C but without an intermediate phase. The sample with $x = 7.5$ belongs to group IV, which has $T_M > T_C$. The sample with $x = 5.0$ falls in group III, in that T_C is expected to be more or less coincident with T_M. We have observed fundamental differences in the behavior of the crystal lattice at the martensitic transition, i.e., stiffening versus softening, determined by the presence or absence of a premartensitic transition and the relation between the Curie temperature and the martensitic-transformation temperature. The elastic and anelastic anomalies reveal the form and strength of coupling of strain with three separate order parameters which combine to give the soft mode, martensitic transition, and ferromagnetic ordering observed in Heusler alloys.

II. EXPERIMENT

The polycrystalline samples of $Ni_{50+x}Mn_{25-x}Ga_{25}$, with a nominal $x = 0$, 2.5, 5.0, and 7.5, were prepared by arc melting

---

*Present address: Dresden High Magnetic Field Laboratory (HLD-EMFL), Helmholtz-Zentrum Dresden-Rossendorf, 01328 Dresden, Germany; c.salazar-mejia@hzdr.de
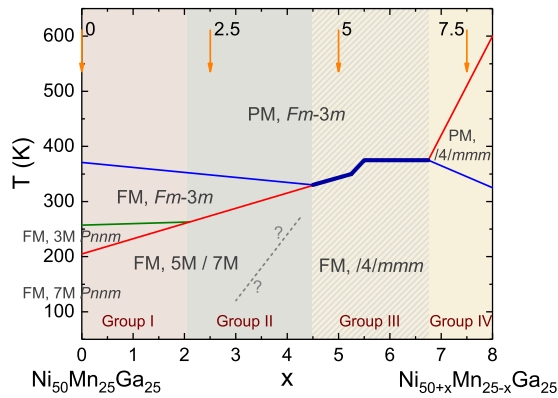†Michael.Nicklas@cpfs.mpg.de

FIG. 1. Schematic phase diagram for the Ni-rich end of the system $Ni_{50+x}Mn_{25-x}Ga_{25}$ (following Refs. [15–18]). The boundary between stability fields of $5M/7M$ martensites and the nonmodulated $I4/mmm$ structure has not yet been determined. Ferromagnetic structures become stable below the blue line (T_C) and martensitic structures become stable below the red line (T_M). The green line is T_{PM}, which marks the transition from the ferromagnetic austenite structure to the premartensite $3M$ structure.

the stoichiometric amounts of the elements under argon atmosphere. The ingots were then enclosed in tantalum ampules under argon atmosphere and, subsequently, sealed in evacuated quartz ampules and homogenized at 1073 K for 3 weeks. Afterwards, they were quenched in cold water. The high quality of the samples was confirmed by x-ray powder diffraction. To ensure homogeneity and confirm the chemical composition, wavelength-dispersive x-ray analysis and light microscopy were used. The actual compositions of the samples have been determined to be $Ni_{50}Mn_{25.5}Ga_{24.5}$, $Ni_{52.5}Mn_{23.25}Ga_{24.25}$, $Ni_{55}Mn_{20.25}Ga_{24.75}$, and $Ni_{57.5}Mn_{18.25}Ga_{24.25}$ for the nominal concentrations $x = 0$, 2.5, 5.0, and 7.5, respectively. In the following, we will denote the samples by their nominal concentrations. Magnetization experiments were carried out in a magnetic properties measurement system (MPMS, Quantum Design). For the RUS investigations, all samples were cut in the form of approximately rectangular parallelepipeds with edge dimensions between 1 and 4 mm. These had masses between 15.1 and 113.6 mg. RUS data were obtained using two different in-house built systems. In the high-temperature instrument, the sample sits lightly between the tips of alumina rods which protrude into a horizontal Netzsch 1600 °C resistance furnace. The piezoelectric transducers are at the other end of the rods, outside the furnace [21]. In the low-temperature instrument, the sample sits directly between the transducers and is suspended in an atmosphere of a few mbars of helium gas, within a helium-flow cryostat [22]. The spectra were collected in the frequency range between 50 and 1200 kHz upon cooling followed by heating in the low-temperature instrument and *vice versa* in the high-temperature instrument. At each set point a period of 20 minutes was allowed for thermal equilibration before the spectrum was collected. The frequency f and width at half-maximum Δf of selected resonance peaks in the primary spectra were fit with an asymmetric Lorentzian function. In general, for a polycrystalline sample, f^2 of each peak scales with some combination of the shear and bulk moduli but, since the resonance modes involve predominantly shearing
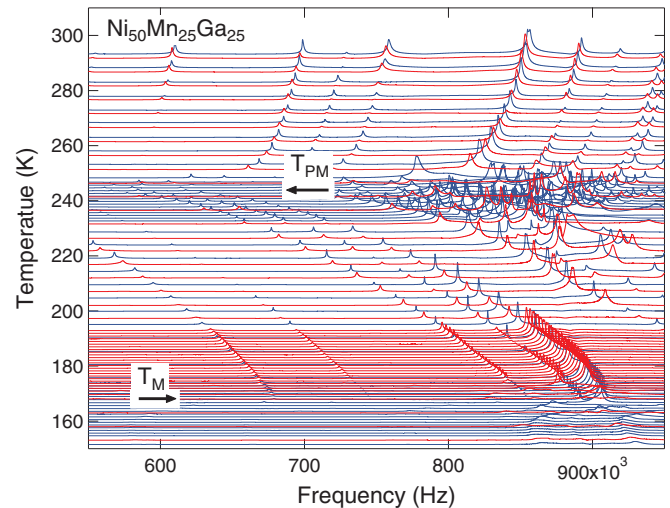

FIG. 2. Segments of RUS spectra for $Ni_{50}Mn_{25}Ga_{25}$. The ordinate is the amplitude of the RUS spectra in arbitrary units. Each spectrum has been offset in proportion to the temperature at which it was collected. Accordingly, the axis is labeled as temperature. Blue traces are spectra collected during cooling and red traces are spectra collected during heating.

motions, the temperature variation of f^2 effectively reflects that of the shear modulus. The inverse mechanical quality factor $Q^{-1} = \Delta f/f$ is a measure of acoustic attenuation.

III. RESULTS

Figure 2 presents segments of RUS spectra for $Ni_{50}Mn_{25}Ga_{25}$ ($x = 0$) in the low-temperature range, recorded during both cooling and heating. $Ni_{50}Mn_{25}Ga_{25}$ orders ferromagnetically at $T_C = 380$ K. On cooling, it undergoes a martensitic transformation at $T_M = 170$ K, which has a hysteresis of about 10 K. Additionally, this sample exhibits a premartensitic transition at $T_{PM} = 246$ K. The dependence of the resonant peaks with temperature can be inferred from the spectra. On cooling from the highest temperatures, a strong shift of the peaks toward lower frequencies (elastic softening) is observed as the temperature approaches the premartensitic transition at T_{PM}. Below this temperature, the peaks shift toward higher frequencies (stiffening) until reaching the martensitic transition at T_M. A marked increase in the width of the peaks and a decrease in the intensity is also evident below T_M. Above T_M, no thermal hysteresis is observed. The temperature dependence of f^2 and of the magnetic susceptibility M/H for $Ni_{50+x}Mn_{25-x}Ga_{25}$ ($x = 0$, 2.5, 5.0, and 7.5) are shown in Fig. 3. The $f^2(T)$ data have been obtained by fitting different resonant peaks, which have been combined by scaling to $f \approx 0.7$, 0.18, 0.18, and 0.58 MHz at room temperature for $x = 0$, 2.5, 5.0, and 7.5, respectively. In general, well-defined peaks have been chosen, in order to be able to trace them in the whole temperature range. Furthermore, peaks at different resonant frequencies have been analyzed to confirm that the shear modulus is frequency independent. Magnetic susceptibility curves were recorded at 200 Oe under cooling and heating protocols. In the following, we will discuss the experimental results in detail.
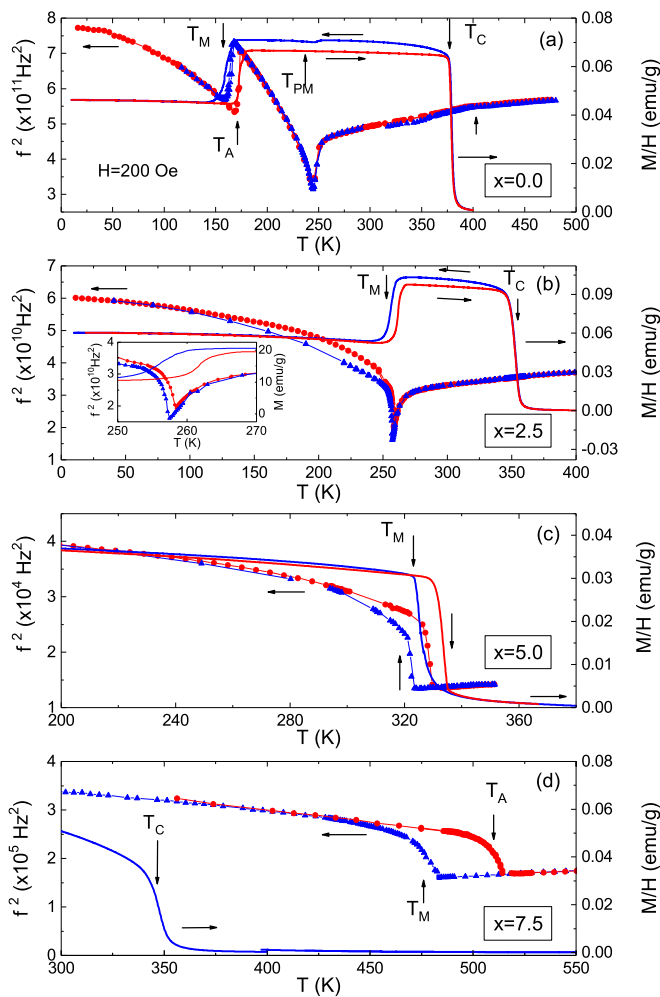
FIG. 3. Temperature dependence f^2 (left axis) and magnetic susceptibility M/H (right axis) for the series $Ni_{50+x}Mn_{25-x}Ga_{25}$ with (a) $x = 0$, (b) 2.5, (c) 5.0, and (d) 7.5. Blue triangles (lines) indicate data recorded on cooling and red circles (lines) on heating. Inset of (b) and (d) show the martensitic transition in detail. Magnetization measurements were performed at 200 Oe.

The magnetic susceptibility of $Ni_{50}Mn_{25}Ga_{25}$ ($x = 0$), displayed in Fig. 3(a), shows three pronounced anomalies. On cooling, the magnetic susceptibility shows an increase at $T_C = 380$ K indicating the ferromagnetic ordering. The pronounced drop in the magnetic susceptibility around $T_M = 170$ K is the result of the martensitic transition at which the crystal structure of the sample changes from cubic to an incommensurate modulated structure [23]. This first-order magnetostructural transition has a hysteresis between cooling and heating cycles ($T_A = 180$ K) of around 10 K. Additionally, a dip at $T_{PM} = 246$ K is observed which corresponds to the premartensitic transition [24–26]. These transitions are reflected in the elastic properties of the material. On cooling from high temperatures, softening of the shear modulus is evident on approaching T_{PM}, with an increase in slope below T_C. A strong dip in $f^2(T)$ is present at T_{PM}, as previously reported [6,27], without thermal hysteresis. Upon further cooling, a trend of stiffening is observed, followed by a steplike softening of about 22% at T_M.

The dominant effect of Ni substitution on the Mn sites in the $Ni_{50+x}Mn_{25-x}Ga_{25}$ series is a shift of the martensitic transition toward higher temperatures and a shift of the ferromagnetic transition toward lower temperatures [15]. Thus, the magnetic susceptibility in $Ni_{52.5}Mn_{22.5}Ga_{25}$ ($x = 2.5$) displays similar behavior to $Ni_{50}Mn_{25}Ga_{25}$ [see Fig. 3(b)]. The transitions move closer together, with T_C decreasing to 353 K and T_M increasing to 256 K, but the premartensitic transition is no longer observed. The elastic properties still show a dip in $f^2(T)$, but this is now located at $T_{M,A}$. Softening is observed as $T \rightarrow T_M$ from above, with a slight increase in slope at T_C. This becomes significantly steeper within 10 K of T_M [inset of Fig. 3(b)] and reverts to strong stiffening below T_M.

Upon further increasing the Ni content, the magnetic susceptibility curves change characteristically. The sample with $x = 5.0$ displays only one transition in $M(T)/H$ [Fig. 3(c)]. Upon cooling, we find a steplike increase in $M(T)/H$ at 325 K, indicating ferromagnetic ordering. At the same time, a hysteresis between heating and cooling cycles marks the first-order character expected for the martensitic transformation. We conclude that in $Ni_{55}Mn_{20}Ga_{25}$ the ferromagnetic and martensitic transitions occur at the same temperature $T_M \approx T_C = 325$ K, i.e., a transition from a paramagnetic-austenitic phase to a ferromagnetic-martensitic phase. The temperature dependence of f^2 exhibits a different pattern than observed for the previous samples with smaller x. Specifically, there is no dip in $f^2(T)$ throughout the whole temperature range. On cooling, a steplike stiffening of the lattice of about 77% is detected at T_M. The stiffening is preceded by weak softening upon approaching T_M from higher temperatures. We note that the slight difference in the transition temperatures determined from RUS and magnetization data might be accounted for by the applied field in case of the latter.

In the sample with the highest Ni content of our investigation, $x = 7.5$, the ferromagnetic transition occurs at $T_C = 345$ K inside the martensitic phase, i.e., $T_C < T_{M,A}$ [see Fig. 3(d)]. The latter takes place at $T_M = 476$ K ($T_A = 510$ K) showing up in $f^2(T)$ as a pronounced stiffening of the lattice of about 145%. The observed hysteresis of 34 K is larger than that observed in the samples with a smaller Ni concentration (ranging from 6 to 12 K). Around $T_{M,A}$ we also observe a small change in paramagnetic susceptibility $M(T)/H$. This reflects the reduction of the effective magnetic moments in the martensitic compared with the austenitic phase [15,28]. The overall temperature dependence of f^2 is similar to that of $Ni_{55}Mn_{20}Ga_{25}$, i.e., slight softening above $T_{M,A}$ followed by a steplike stiffening at the transition and weaker linear stiffening towards lower temperatures. There is no overt change in trend of f^2 at T_C.

The temperature dependencies of the inverse mechanical quality factor Q^{-1}, representing acoustic loss, are plotted for all four samples in Fig. 4. The transitions detected previously in $M(T)/H$ and $f^2(T)$ displayed in Fig. 3 show corresponding anomalies in $Q^{-1}(T)$. $Ni_{50}Mn_{25}Ga_{25}$ exhibits a peak in $Q^{-1}(T)$ at $T_{PM} = 246$ K and steplike changes at T_M and T_A, respectively. There is, perhaps, a slight bump in the data for $Q^{-1}(T)$ at T_C but it is substantially smaller than the clear peaks seen at lower temperatures. $Ni_{52.5}Mn_{22.5}Ga_{25}$ ($x = 2.5$) exhibits a well-pronounced peak in the acoustic loss at $T_{M,A}$. A possible slight anomaly at T_C is again very
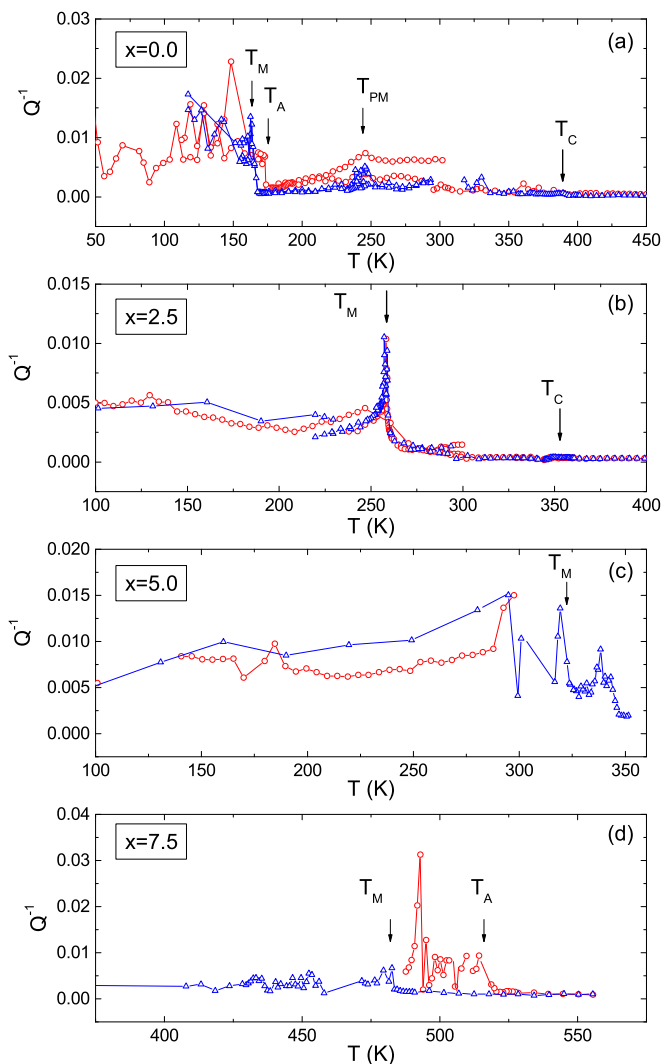
FIG. 4. Temperature dependence of acoustic loss for the samples Ni$_{50+x}$Mn$_{25-x}$Ga$_{25}$ with (a) $x = 0$, (b) $x = 2.5$, (c) $x = 5.0$, and (d) $x = 7.5$. Resonant peaks in the primary spectra remain broad and weak at $T < T_M$, in comparison with those at $T > T_M$. Blue triangles indicate data recorded on cooling and red circles on heating.

small in comparison. The acoustic loss remained higher at all temperatures in the martensitic compared with the austenitic phase. Equivalent data for $x = 5.0$ and 7.5 show a single steep increase in acoustic loss at T_M, to the extent that it was not possible to measure peak widths at temperatures close to the transition point. Peaks in spectra collected from the martensitic phase then remained broad and weak.

IV. DISCUSSION

We note that all investigated samples exhibit a martensitic transformation from a cubic high-temperature austenitic phase to a low-symmetry martensitic phase and a ferromagnetic transition. However, there are substantial differences between the two transitions in the different samples that lead to distinct strain relaxation behavior. These differences are a reflection of the ways that three instabilities combine in Heusler compounds more generally. In the following, we address such differences

from the perspective of how three discrete order parameters couple with strain and with each other, starting with an analysis of the fundamental constraints of symmetry.

A. Group theory

Changes in elastic properties associated with phase transitions occur as a consequence of coupling of strain with the driving order parameter(s). In dynamic measurements, additional anelastic effects are typically due to fluctuations related to the order parameter(s) or of strain relaxation accompanying the motion of defects such as ferroelastic twin walls.

In the case of Ni-Mn-Ga alloys, there are three order parameters to consider, with symmetry properties that are taken here from a more comprehensive symmetry analysis of martensitic transitions [29]. The ferromagnetic transition can be treated, in the simplest case, as having a single order parameter Q_M. The martensitic transitions are more complicated because they involve combinations of an electronic instability [30,31] and a soft mode [24,32,33]. The order parameter for the electronic instability has the symmetry properties of the zone center irreducible representation Γ_3^+ of parent space group $Fm\bar{3}m$. By itself this would give the nonmodulated (NM), tetragonal structure which has space group $I4/mmm$ (e.g., Ref. [34]) and a single order parameter Q_E. The order parameter for the soft mode has symmetry properties related to points along the Σ line between Γ and N of the cubic Brillouin zone, i.e., along a $\langle 110 \rangle^*$ direction. In the simplest case, this can also be expressed using a single order parameter Q_S conforming to Σ_2 symmetry, though it has Γ_3^+ and Γ_5^+ as secondary irreducible representation.

If Q_S operates on its own, the resultant structure is the incommensurate premartensite which is commonly referred to as being the 3M structure. The commensurate equivalent would have space group $Pnnm$ [31,35]. The 7M martensite structure of Ni$_{50}$Mn$_{25}$Ga$_{25}$ arises as a consequence of coupling between Q_E and Q_S. It has space group $Pnnm$ [31,36], though it has also been proposed that the long repeat is incommensurate [23,35]. A 5M structure can occur in Ni$_{50+x}$Mn$_{25-x}$Ga$_{25}$ when x is small (e.g., Refs. [16,18]) and the 5M and 7M structures have both been observed at $x = 4$ [37]. Their stability limits have not yet been fully established.

Order-parameter combinations in structures which occur during heating and cooling of the four Ni-Mn-Ga alloys used in this study can be set out on the basis of the schematic phase diagram introduced in Fig. 1. The sequences of magnetic and structural states and of the order parameters are summarized on Table I.

B. Strain coupling

The form of elastic softening or stiffening associated with each transition will depend on the form of coupling between individual strains and the three driving order parameters, the strength of coupling in each case, and the thermodynamic character of the separate transitions. It has already been shown that the elastic properties of Ni-Mn-Ga alloys measured at frequencies of ~1 Hz show distinct general patterns of elastic softening/stiffening and acoustic loss, which reflect the different groups distinguished by their relative values of T_C and T_M [7,8]. Our present RUS data in combination with data

TABLE I. Sequences of magnetic and structural states for the investigated samples of $Ni_{50+x}Mn_{25-x}Ga_{25}$ upon cooling.

x	Magnetic order	Structure	Q
0	para	$Fm\bar{3}m$	$Q_M = Q_S = Q_E = 0$
	ferro	$Fm\bar{3}m$	$Q_M \neq 0, Q_S = Q_E = 0$
	ferro	$3M$ incommensurate	$Q_M \neq 0, Q_S \neq 0, Q_E = 0$
	ferro	$7M\ Pnnm$	$Q_M \neq 0, Q_S \neq 0, Q_E \neq 0$
2.5	para	$Fm\bar{3}m$	$Q_M = Q_S = Q_E = 0$
	ferro	$Fm\bar{3}m$	$Q_M \neq 0, Q_S = 0, Q_E = 0$
	ferro	$5M$ or $7M\ Pnnm$	$Q_M \neq 0, Q_S \neq 0, Q_E \neq 0$
5.0	para	$Fm\bar{3}m$	$Q_M = Q_S = Q_E = 0$
	ferro	$I4/mmm$	$Q_M \neq 0, Q_S = 0, Q_E \neq 0$
7.5	para	$Fm\bar{3}m$	$Q_M = Q_S = Q_E = 0$
	para	$I4/mmm$	$Q_M = 0, Q_S = 0, Q_E \neq 0$
	ferro	$I4/mmm$	$Q_M \neq 0, Q_S = 0, Q_E \neq 0$

FIG. 5. Variations of the change in $f^2(T)$, $\Delta f^2(T)$, with respect to a linear baseline fit to data in Fig. 3 at $T > T_C$ for $x = 0$ and 2.5. $\Delta f^2(T)$ is expected to scale with the square of the ferromagnetic order parameter, but its magnitude clearly reduces with increasing x.

from the literature allow the underlying causes of these to be set out more explicitly.

Acoustic resonances of a small sample of typical metal or ceramic are determined predominantly by shearing so that f^2 for each resonance mode scales effectively with the shear modulus. For a cubic crystal, this in turn depends on the single-crystal elastic constants C_{44} and $C_{11} - C_{12}$. For the orthorhombic crystals, the shear modulus will depend on the related shear elastic constants and will show the influence, in particular, of changes in C_{66} due to coupling of the order parameters with the shear strain e_6 (see Appendix for details), which arises from irreducible representation Γ_5^+, and in $C_{11} - C_{12}$ due to coupling with the tetragonal shear strain e_t, which arises from irreducible representation Γ_3^+.

The ferromagnetic transition at about 370 K in groups I and II alloys ($x = 0$ and 2.5 in this study) would be expected to give a break in crystallographic symmetry such that the lattice geometry becomes tetragonal due to coupling of the form $\lambda e_t Q_M^2$. This would be expected to give rise to a steplike softening at T_C [38]. This is not observed, however, because the coupling coefficient is sufficiently small that the crystals remain metrically cubic [31]. The observed slight softening must arise from the next highest coupling terms $\lambda e_t^2 Q_M^2$ and $\lambda e_4^2 Q_M^2$ which will give softening or stiffening (depending on the sign of the coupling coefficient λ) proportional to Q_M^2.

Changes in the shear modulus, expressed as the difference Δf^2 between observed values of f^2 and a linear extrapolation of their values from above T_C, are shown in Fig. 5. On this basis, the ferromagnetic transition is thermodynamically continuous and, as in the case of $Ni_{50}Mn_{35}In_{15}$ [4], the effect is small. RUS measurements on a single crystal of $Ni_{50}Mn_{25}Ga_{25}$ have previously shown that a significant contribution to the softening comes from $C_{11} - C_{12}$ [10,13,39,40], but the contribution from C_{44} is not yet known. The magnitude of softening is less at $x = 2.5$ than at $x = 0$ (see Fig. 5), suggesting that the coupling coefficient for $\lambda e_t^2 Q_M^2$ reduces with increasing x. Similar softening would be expected in association with the ferromagnetic transition in group IV alloys, but there is no obvious deviation in f^2 below $T_C = 345$ K in data from the $x = 7.5$ sample [see Fig. 3(d)], implying that the strain
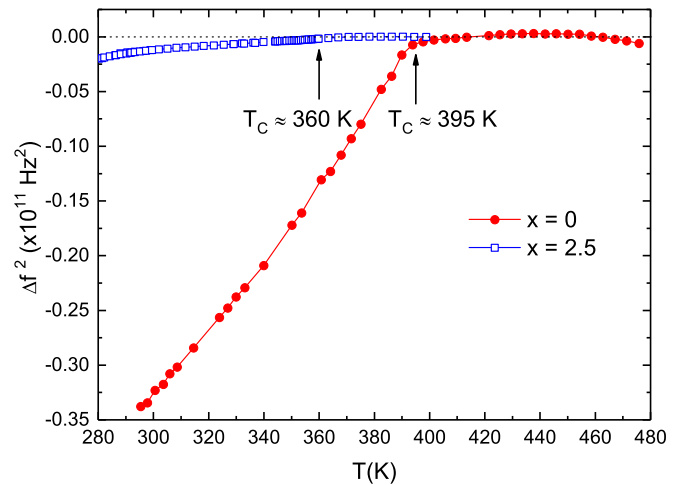
coupling coefficients become negligibly small. An estimation of the magnitudes of symmetry-breaking shear strains can be found in the Appendix.

C. Elastic softening and stiffening

Q_E and $e_1 - e_2$ have the symmetry properties of irreducible representation Γ_3^+ so that bilinear coupling of the form $\lambda(e_1 - e_2)Q_E$ is allowed. This gives rise to softening with falling temperature of $C_{11} - C_{12}$ as the martensitic transition is approached from above, typical of pseudoproper ferroelastic behavior. Single-crystal measurements on stoichiometric $Ni_{50}Mn_{25}Ga_{25}$ at temperatures above T_{PM} have shown this softening and, as expected because e_6 transforms as Γ_5^+ to give coupling of the form $\lambda e_6 Q_E^2$, no equivalent softening was seen in C_{44} [14,41]. The softening seen in $f^2(T)$ for all four samples studied here arises from $C_{11} - C_{12}$, therefore.

The transition from austenite to $3M$ premartensite intervenes before the transition driven by Q_E occurs. This is driven by the Σ_2 order parameter Q_S, with which the strains from the irreducible representations Γ_3^+ and Γ_5^+ couple as $\lambda(e_1 - e_2)Q_S^2$ and $\lambda e_6 Q_S^2$. No latent heat or structural discontinuity which would imply first-order character for the transition has been yet observed [32,42,43], and the heat-capacity anomaly reported in Ref. [43] for a crystal with nearly stoichiometric composition ($x = 0$) has a step at T_{PM} consistent with the transition being second order. A small hysteresis has been reported in magnetic susceptibility and dynamical mechanical analysis (DMA) data for samples of $Ni_{50+x}Mn_{25-x}Ga_{25}$ with $0 \leqslant x \leqslant 2$ [27], but is probably accounted for by the effect of applied magnetic and stress fields. The transition is thus second order and improper ferroelastic, which is expected to give a stepwise softening of both $C_{11} - C_{12}$ and C_{66} [38].

Essentially, this pattern is seen in $C_{11} - C_{12}$ and C_{44} from pulse-echo ultrasonic data for single crystals of $Ni_{50}Mn_{25}Ga_{25}$ [41,43–45]. The frequency of the measurements was not always specified but is assumed to be around 10 MHz. More generally, the elastic anomaly at T_{PM} observed in

measurements made at ~ 1 Hz [7] and 10^5–10^6 Hz, this study, and Refs. [5,6,40], has steep softening in a temperature interval of up to 10 K above the transition point followed by nonlinear recovery below it. The precursor softening is typical of order-parameter fluctuations ahead of improper ferroelastic and coelastic transitions [46,47]. $C_{11} - C_{12}$ recovers to higher values than attained above T_{PM}, which is presumably a consequence of some contribution of bilinear coupling of $e_1 - e_2$ with the Γ_3^+ order parameter, once the cubic symmetry has been broken. The premartensite phase has a tweed microstructure [7,32], so that all these measurements are averages for crystals which may be orthorhombic only on a local length scale [14].

There is no group/subgroup relationship between the premartensite structure and $5M/7M$ martensites. As a consequence, there is no order parameter which relates one directly to the other and the martensitic transition at small values of x is necessarily first order. It is accompanied by a large increase in shear strain and the development of abundant ferroelastic twinning. The elastic anomalies are simply stepwise changes with significant hysteresis and little or no precursor effects [5,6], which is also seen in our data $x = 0$ and 2.5 (group I and II compounds) presented in Figs. 3(a) and 3(b). On the other hand, the austenite-NM transition at larger values of x [group III and IV alloys; $x = 5.0$ and 7.5 data shown in Figs. 3(c) and 3(d)] is driven by the Γ_3^+ order parameter and is first order due to the presence of third-order terms in the Landau expansion for excess free energy. Softening as T_M is approached from above (see Fig. 3) becomes a steep increase in the shear modulus below T_M [8], as expected for pseudoproper ferroelastic character [$\lambda(e_1 - e_2)Q_E, e_6 = 0$] when the transition is first order [38]. The same pattern has been observed at the austenite-$5M/7M$ transition in $Ni_{50}Mn_{35}In_{15}$ [4].

The premartensite and martensite transitions occur at about the same temperature when $x = 2.5$ ($T_{PM} \approx T_M$, see Fig. 1). As a consequence, the variation of $f^2(T)$ displays aspects of both, with the precursor softening due to the proximity to T_{PM} and the recovery below T_M being that of the martensite.

D. Acoustic loss

The patterns of acoustic loss observed by RUS presented in Fig. 4 for the four different Ni-Mn-Ga samples are closely similar to those reported in the literature. In particular, transitions to the premartensitic $3M$ structure and to the NM martensite structure are marked by a sharp peak in attenuation associated with the shear modulus modes at the transition temperatures. The loss peak at T_{PM} has been seen previously in measurements made at 0.1–5 Hz by DMA [8,27], at $\sim$ 1 MHz by RUS [5,6,40], and at 5–10 MHz using pulse-echo ultrasonics [44,45]. The same loss peak was also observed in inverted pendulum experiments [48]. In $Ni_{50+x}Mn_{25-x}Ga_{25}$ with low values of x, at least, the transition is second order in character and the occurrence of the peak always at T_{PM} suggests that the loss mechanism is due to critical slowing down of fluctuations in the order parameter Q_S.

The austenite-NM martensite transition is first order so the loss mechanism is most likely related to the mobility under applied stress of interfaces between the transforming phases. A steep loss peak is typically observed also at the first-order

premartensite-$5M/7M$ transition [8,27], which is again most likely due to mobility of interfaces between coexisting phases. In the case of $Ni_{50}Mn_{25}Ga_{25}$ the temperature interval of coexistence is about 40 K [49], which probably accounts for the broad loss peak seen in this study.

More interesting is the observed loss behavior within the stability fields of the premartensite and martensite phases since this relates to the mobility of ferroelastic twin walls. Under the low-stress conditions of an RUS experiment, Q^{-1} remains relatively high below T_M at compositions which fall within all four alloy groups [47], i.e., for both $5M/7M$ and NM martensites, but reduces to low values in the stability field of the premartensite $3M$ phase [5,6,40]. This is also seen in our study. The same has been reported in some [8], but not all, DMA measurements [27] and in pulse-echo ultrasonic results [45]. The most likely explanation of the difference is that shear strains are also very much smaller in the premartensite structure than in the $5M/7M$ and NM martensites and that, as a consequence, the changes in strain state that occur when a twin wall is displaced are correspondingly much smaller. Alternatively, motion of individual twin walls might be jammed due to interactions between them in the tweed microstructure.

A second, broad loss peak has been seen in the stability fields of both $5M/7M$ martensite [8,9] and premartensite [27] as well as for the $x = 2.5$ sample in this study, but these do not resemble the much steeper loss peaks associated with domain-wall freezing seen, for example, in $LaAlO_3$ [50]. The loss parameters remain high down to the lowest measuring temperatures, suggesting that at least some components of the twin walls remain mobile.

Possible mechanisms for a peak in acoustic loss at the ferromagnetic transition, such as at the antiferromagnetic ordering transition in CoF_2 [51], could include critical slowing down of fluctuations of the magnetic order parameter coupled with phonons. However, any increase in Q^{-1} at T_C of the polycrystalline samples with $x = 0$ and 2.5 appears to be negligibly small in this study. Seiner *et al.* also found no evidence for a loss peak in their RUS data from a slowly cooled single crystal of $Ni_{50}Mn_{25}Ga_{25}$ [40], but they found an increase in Q^{-1} below T_C when a complex microstructure of interacting magnetic domain walls and fine-scale antiphase domains was induced by quenching from high temperatures. This reached a maximum at T_{PM}, suggesting that it was related to the premartensitic transition rather than simply to the ferromagnetic ordering.

E. Order-parameter coupling

As well as each of the three order parameters coupling with strain, it is inevitable that they will couple with each other, either directly or via the common strain. Direct coupling terms allowed by symmetry include $\lambda Q_E Q_S^2$, $\lambda Q_E Q_M^2$, and $\lambda Q_M^2 Q_S^2$. Biquadratic coupling is always allowed and can lead to sequences of structural states involving only one order parameter or both in standard patterns [52]. The consequences of linear-quadratic coupling have only been recently considered in general terms [53], and the predicted structural sequences match aspects of the relationships between structures in Fig. 1. In particular, for $T_{PM} > T_M$, the expected sequence would be a second-order transition to a state with $Q_S \neq 0$, $Q_E = 0$

TABLE II. Expressions used to estimate tetragonal and orthorhombic shear strains, e_t and e_6, in terms of lattice parameters for commensurate $7M$, $3M$, and NM structures. The $3M$ structure is actually incommensurate so, in practice, the commensurate repeat distance for b is taken from the pseudocubic lattice parameters of the orthorhombic structure. Reference axes X, Y, and Z have been taken as parallel to the crystallographic axes of the parent cubic structure which has lattice parameter a_0.

$7M$	$3M$	NM
$e_1 + e_2 = \frac{\sqrt{2}a - a_o}{a_o} + \frac{(\sqrt{2}/7)b - a_o}{a_o}$	$e_1 + e_2 = \frac{\sqrt{2}a - a_o}{a_o} + \frac{(\sqrt{2}/3)b - a_o}{a_o}$	$e_1 = e_2 = \frac{\sqrt{2}a - a_o}{a_o}$
$e_3 = \frac{c - a_o}{a_o}$	$e_3 = \frac{c - a_o}{a_o}$	$e_3 = \frac{c - a_o}{a_o}$
$e_t = \frac{1}{\sqrt{3}}(2e_3 - e_1 - e_2)$	$e_t = \frac{1}{\sqrt{3}}(2e_3 - e_1 - e_2)$	$e_t = \frac{1}{\sqrt{3}}(2e_3 - e_1 - e_2)$
$e_6 = \frac{(\sqrt{2}/7)b - a_o}{a_o} - \frac{\sqrt{2}a - a_o}{a_o}$	$e_6 = \frac{(\sqrt{2}/3)b - a_o}{a_o} - \frac{\sqrt{2}a - a_o}{a_o}$	$e_6 = 0$
$a_o \approx \left(\frac{2}{7}abc\right)^{1/3}$	$a_o \approx \left(\frac{2}{3}abc\right)^{1/3}$	$a_o \approx (2abc)^{1/3}$

followed by a first-order transition to a state with $Q_S \neq 0$, $Q_E \neq 0$. For $T_{PM} < T_M$, a single phase transition to a state with $Q_S \neq 0$, $Q_E \neq 0$ is expected because Q_E acts as a field for Q_S. This is exactly the change seen as T_{PM} and T_M converge with increasing x, and the same arguments apply to the convergence of T_C and T_M.

V. CONCLUSIONS

Combined elasticity and magnetic susceptibility measurements from a set of representative samples belonging to the series $Ni_{50+x}Mn_{25-x}Ga_{25}$ ($x = 0$, 2.5, 5.0, and 7.5) have provided a coherent picture of the consequences of strain coupling effects associated with the particular combination of instabilities that is commonly observed in Heusler alloys. These produce characteristic precursor softening of $C_{11} - C_{12}$ over a wide temperature interval due to bilinear coupling of e_t with the electronic order parameter ($\lambda e_t Q_E$, pseudoproper ferroelastic behavior), stepwise softening below T_M due to linear-quadratic coupling of both e_t and e_6 with the order parameter for the structural transition driven by the soft mode ($\lambda e_t Q_S^2$, $\lambda e_6 Q_S^2$, improper ferroelastic behavior), and biquadratic coupling of e_t and e_4 with the ferromagnetic order parameter ($\lambda e_t^2 Q_M^2$, $\lambda e_4^2 Q_M^2$). The strength of coupling is very substantially greatest for coupling of e_t with Q_E, giving rise to the large shear strains typical of martensitic phase transitions. Coupling of these three order parameters can account for the topology of the phase diagram, as well as for the particular structure types which are observed in Ni-Mn-Ga alloys. Under the low-stress and high-frequency

conditions of an RUS experiment, acoustic losses occur below T_M down to the lowest temperatures at which measurements were made. These have been assumed to relate to mobility of some component of the ferroelastic twin walls, without any indication that they become frozen or pinned.

APPENDIX: SYMMETRY-BREAKING SHEAR STRAINS

The magnitudes of symmetry-breaking shear strains accompanying the premartensite and martensite transitions can be determined from lattice parameter data using the expressions set out in Table II. Representative values of e_t and e_6 calculated from lattice parameters given by Ref. [31] for the $7M$ structure of $Ni_{50}Mn_{25}Ga_{25}$ at 20 K are -0.076 and 0.007, respectively. The value of e_t for a tetragonal nonmodulated structure calculated from the lattice parameters of $Ni_{54.5}Mn_{21.5}Ga_{24}$ at room temperature [48] is 0.217. By way of contrast, the premartensite $3M$ structure has much smaller shear strains, $e_t = -0.007$, $e_6 = 0.002$, as calculated in a related manner using lattice parameters given by Ref. [54] for $Ni_{50}Mn_{25}Ga_{25}$ at 250 K.

[1] A. Sozinov, N. Lanska, A. Soroka, and W. Zou, 12% magnetic field-induced strain in Ni-Mn-Ga-based non-modulated martensite, Appl. Phys. Lett. **102**, 021902 (2013).

[2] O. Heczko, Magnetic shape memory effect and highly mobile twin boundaries, Mater. Sci. Technol. **30**, 1559 (2014).

[3] L. Pareti, M. Solzi, F. Albertini, and A. Paoluzi, Giant entropy change at the co-occurrence of structural and magnetic transitions in the $Ni_{2.19}Mn_{0.81}Ga$ heusler alloy, Eur. Phys. J. B **32**, 303 (2003).

[4] C. Salazar Mejía, A. K. Nayak, J. A. Schiemer, C. Felser, M. Nicklas, and M. A. Carpenter, Strain behavior and lattice dynamics in $Ni_{50}Mn_{35}In_{15}$, J. Phys.: Condens. Matter **27**, 415402 (2015).

[5] V. Sanchez-Alarcos, J. I. Perez-Landazabal, V. Recarte, C. Gomez-Polo, and V. A. Chernenko, Pre-martensitic phenomena in a near stoichiometric Ni_2MnGa polycrystalline alloy, Int. J. Appl. Electrom. Mech. **23**, 93 (2006).

[6] J. I. Perez-Landazabal, V. Sanchez-Alarcos, C. Gomez-Polo, V. Recarte, and V. A. Chernenko, Vibrational and magnetic behavior of transforming and nontransforming Ni-Mn-Ga alloys, Phys. Rev. B **76**, 092101 (2007).

[7] V. A. Chernenko, J. Pons, C. Segui, and E. Cesari, Premartensitic phenomena and other phase transformations in Ni-Mn-Ga alloys studied by dynamical mechanical analysis and electron diffraction, Acta Mater. **50**, 53 (2002).

[8] S. H. Chang and S. K. Wu, Low-frequency damping properties of near-stoichiometric Ni$_2$MnGa shape memory alloys under isothermal conditions, Scr. Mater. **59**, 1039 (2008).

[9] I. Aaltio, M. Lahelin, O. Soderberg, O. Heczko, B. Lofgren, Y. Ge, J. Seppala, and S. P. Hannula, Temperature dependence of the damping properties of Ni-Mn-Ga alloys, Mater. Sci. Eng. A **481**, 314 (2008).

[10] H. Seiner, L. Bicanova, P. Sedlak, M. Landa, L. Heller, and I. Aaltio, Magneto-elastic attenuation in austenitic phase of Ni-Mn-Ga alloy investigated by ultrasonic methods, Mater. Sci. Eng. A **521-522**, 205 (2009).

[11] P. Sedlak, H. Seiner, L. Bodnarova, O. Heczko, and M. Landa, Elastic constants of non-modulated Ni-Mn-Ga martensite, Scr. Mater. **136**, 20 (2017).

[12] O. Heczko, H. Seiner, P. Sedlak, J. Kopecek, V. Kopecky, and M. Landa, Resonant ultrasound spectroscopy–a tool to probe magneto-elastic properties of ferromagnetic shape memory alloys, Eur. Phys. J. B **86**, 62 (2013).

[13] H. Seiner, O. Heczko, P. Sedlak, L. Bodnarova, M. Novotny, J. Kopecek, and M. Landa, Combined effect of structural softening and magneto-elastic coupling on elastic coefficients of Ni-Mn-Ga austenite, J. Alloys Compd. **577S**, S131 (2013).

[14] H. Seiner, V. Kopecky, M. Landa, and O. Heczko, Elasticity and magnetism of Ni$_2$MnGa premartensitic tweed, Phys. Status Solidi B **251**, 2097 (2014).

[15] A. N. Vasil'ev, A. D. Bozhko, V. V. Khovailo, I. E. Dikshtein, V. G. Shavrov, V. D. Buchelnikov, M. Matsumoto, S. Suzuki, T. Takagi, and J. Tani, Structural and magnetic phase transitions in shape-memory alloys Ni$_{2+x}$Mn$_{1-x}$Ga, Phys. Rev. B **59**, 1113 (1999).

[16] A. N. Vasil'ev, V. D. Buchelnikov, T. Takagi, V. V. Khovailo, and E. I. Estrin, Shape memory ferromagnets, Phys. Usp. **46**, 559 (2003).

[17] V. V. Khovaylo, V. D. Buchelnikov, R. Kainuma, V. V. Koledov, M. Ohtsuka, V. G. Shavrov, T. Takagi, S. V. Taskaev, and A. N. Vasiliev, Phase transitions in Ni$_{2+x}$Mn$_{1-x}$Ga with a high Ni excess, Phys. Rev. B **72**, 224408 (2005).

[18] P. Entel, M. E. Gruner, D. Comtesse, V. V. Sokolovskiy, and V. D. Buchelnikov, Interacting magnetic cluster-spin glasses and strain glasses in Ni-Mn based heusler structured intermetallics, Phys. Status Solidi B **251**, 2135 (2014).

[19] V. A. Chernenko, E. Cesari, V. V. Kokorin, and I. N. Vitenko, The development of new ferromagnetic shape memory alloys in Ni-Mn-Ga system, Scr. Metall. Mater. **33**, 1239 (1995).

[20] V. A. Chernenko, Compositional instability of β-phase in Ni-Mn-Ga alloys, Scr. Mater. **40**, 523 (1999).

[21] R. E. A. McKnight, T. Moxon, A. Buckley, P. A. Taylor, T. W. Darling, and M. A. Carpenter, Grain size dependence of elastic anomalies accompanying the alpha-beta phase transition in polycrystalline quartz, J. Phys.: Condens. Matter **20**, 075229 (2008).

[22] R. E. A. McKnight, M. A. Carpenter, T. W. Darling, A. Buckley, and P. A. Taylor, Acoustic dissipation associated with phase transitions in lawsonite, CaAl$_2$Si$_2$O$_7$(OH)(2)·H$_2$O, Am. Mineral. **92**, 1665 (2007).

[23] S. Singh, V. Petricek, P. Rajput, A. H. Hill, E. Suard, S. R. Barman, and D. Pandey, High-resolution synchrotron x-ray powder diffraction study of the incommensurate modulation in the martensite phase of Ni$_2$MnGa: Evidence for nearly 7M modulation and phason broadening, Phys. Rev. B **90**, 014109 (2014).

[24] U. Stuhr, P. Vorderwisch, V. V. Kokorin, and P. A. Lindgard, Premartensitic phenomena in the ferro- and paramagnetic phases of Ni$_2$MnGa, Phys. Rev. B **56**, 14360 (1997).

[25] X. Moya, L. Mañosa, A. Planes, T. Krenke, M. Acet, V. O. Garlea, T. A. Lograsso, D. L. Schlagel, and J. L. Zarestky, Lattice dynamics and phonon softening in Ni-Mn-Al heusler alloys, Phys. Rev. B **73**, 064303 (2006).

[26] X. Moya, D. Gonzalez-Alonso, L. Mañosa, A. Planes, V. O. Garlea, T. A. Lograsso, D. L. Schlagel, J. L. Zarestky, S. Aksoy, and M. Acet, Lattice dynamics in magnetic superelastic Ni-Mn-In alloys: Neutron scattering and ultrasonic experiments, Phys. Rev. B **79**, 214118 (2009).

[27] J. Liu, J. Wang, C. Jiang, and H. Xu, Internal friction associated with the premartensitic transformation and twin boundary motion of Ni$_{50+x}$Mn$_{25-x}$Ga$_{25}$ (x = 0–2) alloys, J. Appl. Phys. **113**, 103502 (2013).

[28] A. V. Korolev, N. I. Kourov, and V. G. Pushin, Specific features of magnetic properties upon martensitic transition $M \longleftrightarrow L2_1$ in Ni$_{2+x}$Mn$_{1-x}$Ga alloys, Phys. Solid State **57**, 316 (2015).

[29] M. A. Carpenter and C. J. Howard (unpublished).

[30] P. J. Brown, A. Y. Bargawi, J. Crangle, K. U. Neumann, and K. R. A. Ziebeck, Direct observation of a band Jahn-Teller effect in the martensitic phase transition of Ni$_2$MnGa, J. Phys.: Condens. Matter **11**, 4715 (1999).

[31] P. J. Brown, J. Crangle, T. Kanomata, M. Matsumoto, B. Ouladdiaf, K. U. Neumann, and K. R. A. Ziebeck, The crystal structure and phase transitions of the magnetic shape memory compound Ni$_2$MnGa, J. Phys.: Condens. Matter **14**, 10159 (2002).

[32] A. Zheludev, S. M. Shapiro, P. Wochner, A. Schwartz, M. Wall, and L. E. Tanner, Precursor effects and premartensitic transformation in Ni$_2$MnGa, Phys. Rev. B **51**, 11310 (1995).

[33] L. Mañosa, A. Planes, J. Zarestky, T. Lograsso, D. L. Schlagel, and C. Stassis, Phonon softening in Ni-Mn-Ga alloys, Phys. Rev. B **64**, 024305 (2001).

[34] S. Banik, R. Ranjan, A. Chakrabarti, S. Bhardwaj, N. P. Lalla, A. M. Awasthi, V. Sathe, D. M. Phase, P. K. Mukhopadhyay, D. Pandey, and S. R. Barman, Structural studies of Ni$_{2+x}$Mn$_{1-x}$Ga by powder x-ray diffraction and total energy calculations, Phys. Rev. B **75**, 104107 (2007).

[35] S. Singh, S. R. Barman, and D. Pandey, Incommensurate modulations in stoichiometric Ni$_2$MnGa ferromagnetic shape memory alloy: An overview, Z. Kristallogr. **230**, 13 (2015).

[36] R. Ranjan, S. Banik, S. R. Barman, U. Kumar, P. K. Mukhopadhyay, and D. Pandey, Powder x-ray diffraction study of the thermoelastic martensitic transition in Ni$_2$Mn$_{1.05}$Ga$_{0.9515}$, Phys. Rev. B **74**, 224443 (2006).

[37] V. V. Khovaylo, K. Oikawa, C. Wedel, T. Takagi, T. Abe, and K. Sugiyama, Influence of intermartensitic transitions on transport properties of Ni$_{2.16}$Mn$_{0.84}$Ga alloy, J. Phys.: Condens. Matter **16**, 1951 (2004).

[38] M. A. Carpenter and E. K. H. Salje, Elastic anomalies in minerals due to structural phase transitions, Eur. J. Mineral. **10**, 693 (1998).

[39] O. Heczko, H. Seiner, P. Sedlak, J. Kopecek, and M. Landa, Anomalous lattice softening of Ni$_2$MnGa austenite due to magnetoelastic coupling, J. Appl. Phys. **111**, 07A929 (2012).

[40] H. Seiner, P. Sedlak, L. Bodnarova, J. Drahokoupil, V. Kopecky, J. Kopecek, M. Landa, and O. Heczko, The effect of antiphase

boundaries on the elastic properties of Ni-Mn-Ga austenite and premartensite, J. Phys.: Condens. Matter **25**, 425402 (2013).

[41] M. Stipcich, L. Mañosa, A. Planes, M. Morin, J. Zarestky, T. Lograsso, and C. Stassis, Elastic constants of Ni-Mn-Ga magnetic shape memory alloys, Phys. Rev. B **70**, 054115 (2004).

[42] V. V. Kokorin, V. A. Chernenko, E. Cesari, J. Pons, and C. Segui, Pre-martensitic state in Ni-Mn-Ga alloys, J. Phys.: Condens. Matter **8**, 6457 (1996).

[43] L. Mañosa, A. González-Comas, E. Obradó, A. Planes, V. A. Chernenko, V. V. Kokorin, and E. Cesari, Anomalies related to the TA_2-phonon-mode condensation in the heusler Ni_2MnGa alloy, Phys. Rev. B **55**, 11068 (1997).

[44] J. Worgull, E. Petti, and J. Trivisonno, Behavior of the elastic properties near an intermediate phase transition in Ni_2MnGa, Phys. Rev. B **54**, 15695 (1996).

[45] T. E. Stenger and J. Trivisonno, Ultrasonic study of the two-step martensitic phase transformation in Ni_2MnGa, Phys. Rev. B **57**, 2735 (1998).

[46] M. A. Carpenter, E. K. H. Salje, A. Graeme-Barber, B. Wruck, M. T. Dove, and K. S. Knight, Calibration of excess thermodynamic properties and elastic constant variations associated with the $\alpha \longleftrightarrow \beta$ phase transition in quartz, Am. Mineral. **83**, 2 (1998).

[47] M. A. Carpenter, Static and dynamic strain coupling behavior of ferroic and multiferroic perovskites from resonant ultrasound spectroscopy, J. Phys.: Condens. Matter **27**, 263201 (2015).

[48] V. G. Gavriljuk, O. Soederberg, V. V. Bliznuk, N. I. Glavatska, and V. K. Lindroos, Martensitic transformations and mobility of twin boundaries in Ni_2MnGa alloys studied by using internal friction, Scr. Mater. **49**, 803 (2003).

[49] S. Singh, J. Bednarcik, S. R. Barman, C. Felser, and D. Pandey, Premartensite to martensite transition and its implications for the origin of modulation in Ni_2MnGa ferromagnetic shape-memory alloy, Phys. Rev. B **92**, 054112 (2015).

[50] R. J. Harrison, S. A. T. Redfern, and E. K. H. Salje, Dynamical excitation and anelastic relaxation of ferroelastic domain walls in $LaAlO_3$, Phys. Rev. B **69**, 144101 (2004).

[51] R. I. Thomson, T. Chatterji, and M. A. Carpenter, CoF_2: A model system for magnetoelastic coupling and elastic softening mechanisms associated with paramagnetic $\longleftrightarrow$ antiferromagnetic phase transitions, J. Phys.: Condens. Matter **26**, 146001 (2014).

[52] E. K. H. Salje and V. Devarajan, Phase transitions in systems with strain-induced coupling between two order parameters, Phase Trans. **6**, 235 (1986).

[53] E. K. H. Salje and M. A. Carpenter, Linear-quadratic order parameter coupling and multiferroic phase transitions, J. Phys.: Condens. Matter **23**, 462202 (2011).

[54] T. Ohba, N. Miyamoto, K. Fukuda, T. Kakeshita, and K. Kato, Fundamental structure of a Ni_2MnGa intermediate phase having an orthorhombic lattice, Smart Mater. Struct. **14**, S197 (2005).